University of Bristol - Explore Bristol Research
General rights

Optical implementation of spin squeezing

You may also be interested in:

New Journal of Physics

The open access journal at the forefront of physics

CrossMark

PAPER

Optical implementation of spin squeezing

Takafumi Ono[1], Javier Sabines-Chesterking, Hugo Cable, Jeremy L O'Brien and Jonathan C F Matthews[1]

Quantum Engineering Technology Labs, H. H. Wills Physics Laboratory and Department of Electrical & Electronic Engineering, University of Bristol, BS8 1FD, United Kingdom

[1]   Authors to whom any correspondence should be addressed.

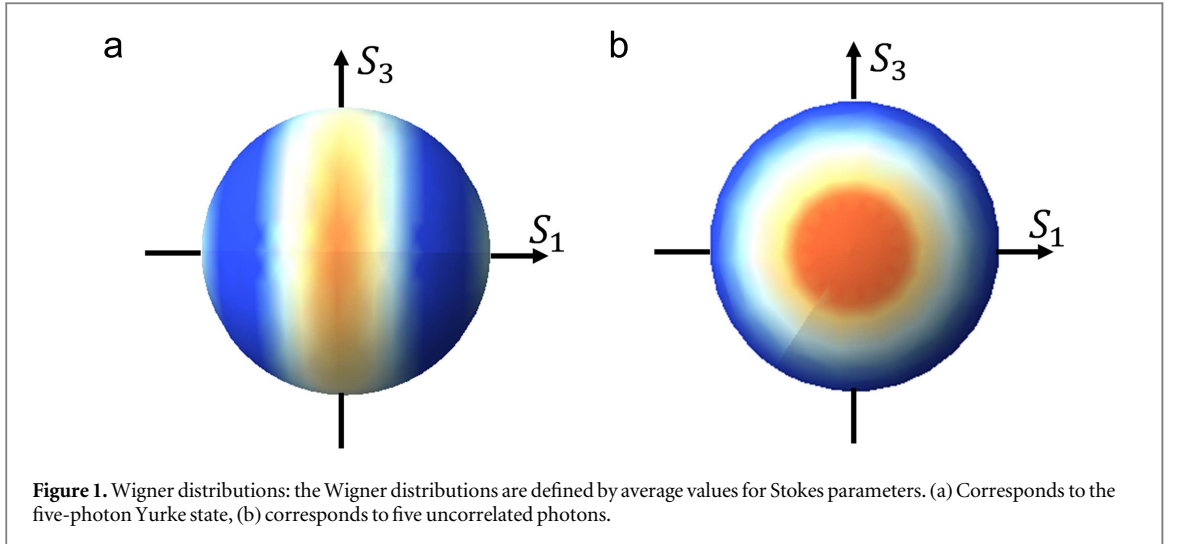**E-mail:** Takafumi.Ono@Bristol.ac.uk and Jonathan.Matthews@Bristol.ac.uk

Abstract

Quantum metrology enables estimation of optical phase shifts with precision beyond the shot-noise limit. One way to exceed this limit is to use squeezed states, where the quantum noise of one observable is reduced at the expense of increased quantum noise for its complementary partner. Because shot-noise limits the phase sensitivity of all classical states, reduced noise in the average value for the observable being measured allows for improved phase sensitivity. However, additional phase sensitivity can be achieved using phase estimation strategies that account for the full distribution of measurement outcomes. Here we experimentally investigate a model of optical spin-squeezing, which uses post-selection and photon subtraction from the state generated using a parametric down-conversion photon source, and we investigate the phase sensitivity of this model. The Fisher information for all photon-number outcomes shows it is possible to obtain a quantum advantage of 1.58 compared to the shot-noise value for five-photon events, even though due to experimental imperfection, the average noise for the relevant spin-observable does not achieve sub-shot-noise precision. Our demonstration implies improved performance of spin squeezing for applications to quantum metrology.

1. Introduction

Quantum metrology uses non-classical states to enable measurement of physical parameters with precision beyond the fundamental shot-noise limit [1]. This is subject to intense research effort for measurements at the single-photon level [2], with higher intensity quantum optics [3] and with matter [4]. In all these cases the central motivation is to understand how to extract more information per-unit of resource (such as probe power and interaction time) and this will naturally lead to applications in precision measurement [5–8]. An approach that dates back to the beginning of quantum optics [9] is to improve phase sensitivity using squeezed states [3]. In discrete quantum optics, one approach has been to use path-entangled states, such as NOON states [10], as a means to achieve supersensitivity since they exhibit interference patterns with increased frequency compared to classical light. So far, experiments have reached photon numbers of up to six [11–13] photons, and recent works aim to address weaknesses in these schemes due to loss [14] and state generation using non-deterministic processes [15]. Using probes multiple times can also enable a precision advantage, which varies according to the chosen notion of resource [16, 17].

Spin squeezing has proven to be a useful approach thanks to developments in experiments manipulating atomic ensembles [18–23]. In these experiments ensemble measurements are typically used, which correspond to collective observables for all particles in the ensemble. However, experiments that utilise detections at the single-particle level, can in principle achieve sensitivity beyond that achievable using ensemble measurements [24]. The total statistical information that can be extracted from a measurement of an unknown phase shift is captured by the Fisher information [25, 26], which is evaluated for all measurement outcomes. Because it is well known that squeezing can improve the phase sensitivity in many set-ups, it is important to quantify the

Figure 1. Wigner distributions: the Wigner distributions are defined by average values for Stokes parameters. (a) Corresponds to the five-photon Yurke state, (b) corresponds to five uncorrelated photons.

sensitivity improvement with squeezing, and how close this sensitivity is to the maximum phase sensitivity as quantified using Fisher information.

In this paper, we focus on measurements using spin squeezing [27, 28], which has been shown to enable increased sensitivity in several experiments using ultracold atoms [29–32]. We report on an optical implementation of a spin-squeezing model which was originally considered by Yurke *et al* [33, 34], and we investigate how sensitivity is improved in this model. Our setup generates five-photon Yurke states by postselecting on cases with five detection events from the state emitted by a parametric downconversion source after one photon subtraction [35], and we use spatially-multiplexed pseudo-number-resolving detection to reconstruct photon-number statistics at the output [15]. Our analysis demonstrates increased sensitivity from the observed optical Yurke state, using all five-photon coincidence outcomes. We investigate the role of spin squeezing in achieving this quantum enhancement by using our optical spin-squeezing model.

Consider first N uncorrelated single photons, where each photon is in a superposition of horizontal (H) and vertical (V) polarisations, $(|1, 0\rangle_{HV} + |0, 1\rangle_{HV})/\sqrt{2}$. When we measure this state in HV-polarisation basis, the probability that n photons are detected with H polarisation and $N - n$ photons with V polarisation is given by the Binomial distribution $P_n = \binom{N}{n}(1/2)^N$. The noise obtained from this distribution is given by $\sqrt{N}$, which is called shot noise for phase estimation.

The state which we consider here, sometimes referred to as the Yurke state [33], is a superposition of the two states of $(N + 1)/2$ photons are in one optical mode (e.g. horizontal polarisation) and $(N + 1)/2 - 1$ photons are in an orthogonal mode (e. g. vertical polarisation) of the form $(|(N - 1)/2, (N + 1)/2\rangle + |(N + 1)/2, (N - 1)/2\rangle)/\sqrt{2}$, where $N \geqslant 3$ is restricted to odd values. If we adopt polarisation encoding and measure in the HV basis, the outcomes take two values with photon-number difference ± 1. The noise of Yurke state is therefore 1 which is smaller than that using N uncorrelated photons with a noise of $\sqrt{N}$.

More generally, the photon statistics of any two-mode N-photon system can be described by the Stokes parameters describing the photon-number differences between H and V polarisation, diagonal (D) and anti-diagonal (A) polarisation, and right-circular (R) and left-circular (L) polarisation,

$$\hat{S}_1 = \hat{n}_H - \hat{n}_V = \hat{a}_H^\dagger \hat{a}_H - \hat{a}_V^\dagger \hat{a}_V,$$
$$\hat{S}_2 = \hat{n}_D - \hat{n}_A = \hat{a}_H^\dagger \hat{a}_V + \hat{a}_V^\dagger \hat{a}_H,$$
$$\hat{S}_3 = \hat{n}_R - \hat{n}_L = -i(\hat{a}_H^\dagger \hat{a}_V - \hat{a}_V^\dagger \hat{a}_H),$$

where $\hat{a}_i^\dagger$, $\hat{a}_i$ and $\hat{n}_i$ are the creation, annihilation and number operators for the corresponding modes. The average of these parameters, $\mathbf{S} = (\langle\hat{S}_1\rangle, \langle\hat{S}_2\rangle, \langle\hat{S}_3\rangle)$, is $\mathbf{S} = (0, N, 0)$ for uncorrelated photons and $\mathbf{S} = (0, (N + 1)/2, 0)$ for the Yurke state, indicating that these vectors align with the S_2 axis of the Poincare sphere.

The squeezing property of the Yurke state can be described using $\hat{S}_1$ and $\hat{S}_3$. For N uncorrelated photons, the noise for S_1 and S_3 is equivalent, $\Delta S_1 = \Delta S_3 = \sqrt{N}$ (figure 1(b)). On the other hand for the Yurke state, the noise of S_1 is suppressed as $\Delta S_1 = 1$ at the expense of increased noise S_3, $\Delta S_3 = \sqrt{(N^2 + 2N - 1)/2}$ (figure 1(a)). A large number of parameters have been devised to quantify spin squeezing for various applications [28]. To characterise this squeezing, we use the squeezing parameter, ξ_S, which is defined to be the ratio between the minimum uncertainty for directions orthogonal to $\mathbf{S}$ [27], where $\xi_S < 1$ indicates reduced quantum noise

below the shot-noise. For uncorrelated photons, $\xi_S = 1$. While for the Yurke state, ξ_S is minimised along the S_1 direction with $\xi_S = 1/\sqrt{N}$ which indicates strong squeezing for this choice of squeezing parameter.

The squeezing property of the Yurke state can be used for improving the phase sensitivity of an interferometer. The effect of a phase rotation by ϕ can be described by the unitary operator $\hat{U}(\phi) = \exp(-i\hat{S}_3\phi/2)$. Specifically, $\hat{S}_1$ after the phase rotation is expressed as $\hat{S}_1(\phi) = \hat{U}^\dagger(\phi)\hat{S}_1\hat{U}(\phi) = \cos(\phi)\hat{S}_1 - \sin(\phi)\hat{S}_2$. Because $\langle\hat{S}_1\rangle = 0$ for both N uncorrelated photons and the Yurke state, the average of $\hat{S}_1(\phi)$ is expressed by

$$\langle\hat{S}_1\rangle(\phi) = -\langle\hat{S}_2\rangle\sin(\phi). \tag{1}$$

For estimates of $\hat{S}_1$, phase error is given by the ratio of ΔS_1 and the phase derivative of $\langle\hat{S}_1\rangle$. Specifically, the phase error at $\phi = 0$ is given by

$$\delta\phi_{\mathrm{sq}} = \Delta S_1 / |\partial\langle\hat{S}_1\rangle/\partial\phi||_{\phi=0} = \frac{\Delta S_1}{\langle\hat{S}_2\rangle}. \tag{2}$$

Because $\Delta S_1 = 1$ and $\langle\hat{S}_2\rangle = (N+1)/2$ for the Yurke state, the phase error by squeezing of Yurke state is $\delta\phi_{\mathrm{sq}} = 2/(N+1)$. To characterise the improvement of the phase sensitivity due to squeezing, we use another squeezing parameter ξ_R which was introduced in [36, 37], which is the ratio of the phase error for a general state and phase error due to shot noise $\delta\phi_{\mathrm{SNL}} = 1/\sqrt{N}$, with $\xi_R = \delta\phi_{\mathrm{sq}}/\delta\phi_{\mathrm{SNL}}$. For $\xi_R < 1$, the phase error is smaller than the shot-noise limit attained by uncorrelated photons $\xi_R = 1$. For the Yurke state, $\xi_R = 2\sqrt{N}/(N+1) \approx 2/\sqrt{N} < 1$ for the high-N limit.

Although squeezing of the Stokes parameters can improve phase sensitivity beyond the shot-noise limit, additional phase sensitivity can be achieved by phase estimation which accounts for the full distribution of measurement outcomes. Statistical information about ϕ can be extracted from the frequencies of every measurement outcome occurring in an experiment and quantified using Fisher information $F(\phi)$. In a two-mode N-photon problem, Fisher information is calculated from the $N+1$ probability distributions, $p_m(\phi)$, where m photons are detected with H polarisation and $N-m$ photons with V polarisation

$$F(\phi) = \sum_{m=0}^{N} p_m(\phi)\left(\frac{\partial}{\partial\phi}\ln p_m(\phi)\right)^2. \tag{3}$$

More specifically, the Cramér–Rao bound states that any unbiased statistical estimator of ϕ has mean-square error which is lower bounded by $1/F(\phi)$, and this bound can be saturated using a suitable statistical estimator [38]. The minimum phase error for the Yurke state is then given by $\delta\phi_{\mathrm{opt}} = 1/\sqrt{F} = 1/\sqrt{(N^2 + 2N - 1)/2}$, where we used $F = \Delta^2 S_3$ [39]. The improvement factor compared to the shot-noise limit is $\delta\phi_{\mathrm{opt}}/\delta\phi_{\mathrm{SNL}} \approx \sqrt{2}/\sqrt{N}$ for the high-N limit. Note that the phase sensitivity obtained from the Fisher information is greater than the sensitivity obtained from equation (2) by a factor of approximately $\sqrt{2}$, indicating that maximum sensitivity is achieved not only due to squeezing but also other quantum effects captured by the full set of measurement outcomes. Note that a theoretical analysis with similar motivation is given in [24].

2. Experimental setup

In order to demonstrate experimentally the phase sensitivity obtained from squeezing and maximum phase sensitivity obtained from Fisher information, we have implemented a five-photon Yurke state model by using a post-selection technique. Figure 2 shows the experimental setup for generating the Yurke state. Down-converted photon pairs are generated from biaxial Type-I bismuth borate (BiBO) crystal in a non-collinear configuration. A half wave plate (HWP) is placed on each path so that one path is horizontally polarised and the other is vertically polarized. Each beam is then combined into a single spatial mode at the polarisation beam splitter (PBS1). The state after the PBS1 is a superposition of photon number states with equal photon number in the horizontal and vertical polarisation,

$$|\Psi_{\mathrm{PDC}}\rangle = \frac{1}{\cosh r}\sum_{N=0}^{\infty}(\tanh r)^{N/2}|N/2, N/2\rangle_{\mathrm{HV}}, \tag{4}$$

where the sum is taken over even values of N. If we postselect N photons from this state, the state is equivalent to the Holland–Burnett state $|N/2, N/2\rangle_{\mathrm{HV}}$ [13].

To generate the Yurke state [35], one photon is subtracted from the down-converted photon source, by detection of a single-photon in the D/A basis. After the one-photon subtraction, the conditional output is the five-photon Yurke state. In the setup, we put a beam splitter after PBS1 so that each of the N photons in the beam is transmitted with probability 10%. The transmitted one-photon state was measured in the D/A basis using a

Figure 2. Experimental set-up. Ultraviolet laser pulses, with a central wavelength of 404 nm from a frequency-doubled mode-locked Ti:sapphire laser (wavelength: 808 nm, pulse width: 100 fs, repetition rate 80 MHz), pump a 2 mm thick biaxial Type-I bismuth borate (BiBO) crystal. A dichroic mirror transmits the down-converted light and reflects the pump beam. The signal and idler photons are rotated to 3° with respect to the pump beam. The arrival timing between the signal and idler photons at PBS1 is adjusted by using a translation stage. After PBS1, a 3 nm bandwidth band-pass filter is used to remove the fluorescent light. BS: non-polarising beamsplitter with 10% transmission. BPF: bandpass filter. PBS3 measures in the diagonal polarisation basis.

HWP set at 22.5° and PBS3. After the one-photon detection, the reflected $N - 1$ photons are analysed by the polarisation interferometer.
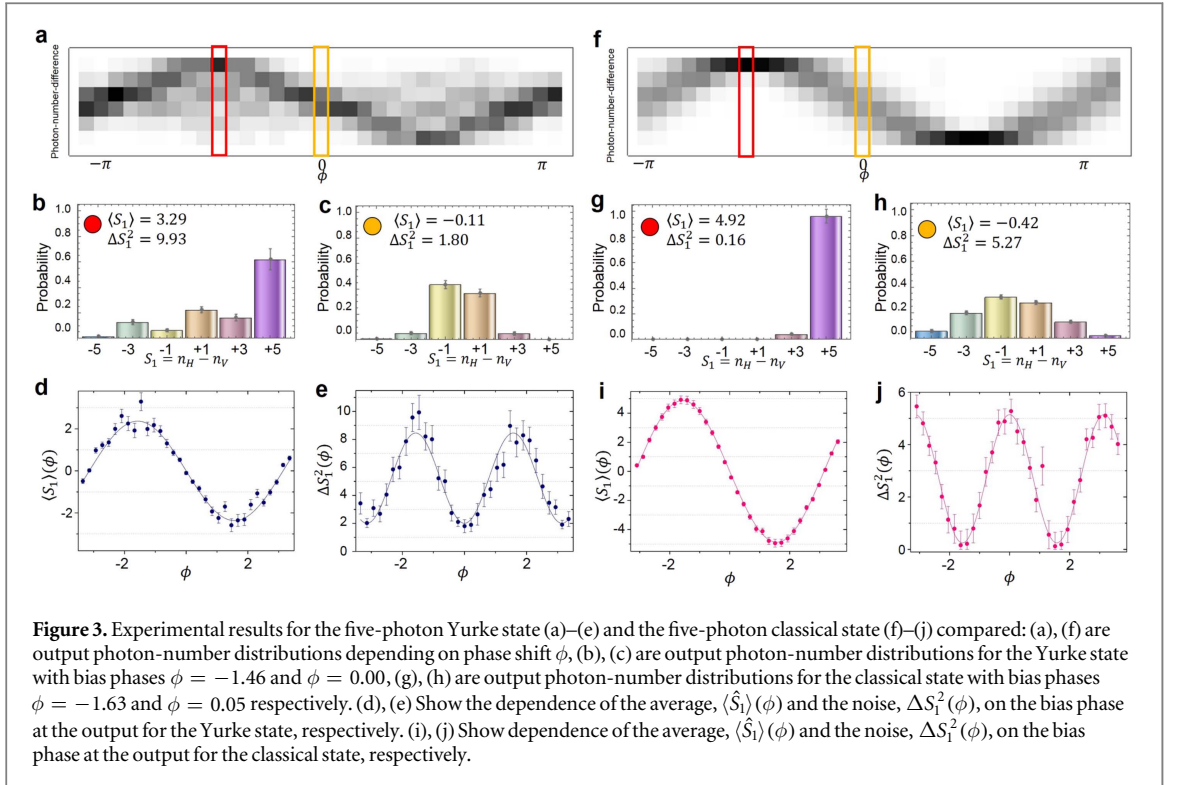
Note that the conditional output state after the one photon subtraction is the superposition of arbitrary (odd) photon-number Yurke states, since the down-converted photon state is the superposition of even-photon number states described in equation (4). Typical count rates for two, four, six-fold coincidence are 7×10^5, 40 and 10^{-2} Hz, respectively. In this experiment, we only focus on cases with five detection events after the one-photon subtraction.

To demonstrate the sub-shot noise phase measurement, we measured all possible coincidence outcomes, of which there are six, at the output as ϕ is varied. We used a pseudo-number-resolving multiplexed detection system using 1×7 fibre beam splitters, 14 avalanche photodiodes (APDs) and a multi-channel photon correlator (DPC-230, Becker and Hickl GmbH) [15]. The phase shift was measured by using a HWP and PBS3 which were placed on the reflected path of the beam splitter.

Details of measurement times and efficiency for our experiment are as follows. For our six-photon measurements, data collection took eight hours per point in the interference fringe. Quantum efficiencies of our APDs are roughly 55% at 808 nm. Transmittance through the all the optical components including coupling efficiency from free space to fibre is estimated as 20%. The reflectivity of the non-polarising beamsplitter is 90%. Assuming equal splitting probability amongst the seven detectors at each interferometer output, the efficiency for detecting five-photon outcomes ranges from 15% to 52%. Hence, overall efficiency can be estimated as $0.55 \times 0.2 \times 0.9 \times 0.15 \approx 0.014$.

3. Results

Figure 3 shows experimentally-obtained Yurke state interference (figures 3(a)–(e)) and shot-noise limited interference (figures 3(f)–(j)). Figures 3(a) and (f) show the effect on S_1 for the Yurke state and uncorrelated photons as ϕ is varied. As expected from equation (1), the averages of the probability distributions follow the sine-pattern. The output noise in figure 3(a) is clearly reduced at around $\phi = 0$ where the squeezing sensitivity is maximum, whereas the noise in figure 3(f) is limited by shot noise. Figures 3(b), (c), (g) and (h) show the probability distributions for specific bias phases where the averages values of S_1 are nearly maximum (figures 3(b) and (g)) and are nearly zero (figures 3(c) and (h)) respectively. It can be seen from figure 3(b) that the effect of two photon coherence appears as the photon-number oscillation for Yurke state [40] (the peaks are observed at $S_1 = -3, +1$ and $+5$), and results in the reduced quantum noise at the phase where the average is nearly zero (figure 3(c)). On the other hand, for the classical uncorrelated case, the probability distribution of a

Figure 3. Experimental results for the five-photon Yurke state (a)–(e) and the five-photon classical state (f)–(j) compared: (a), (f) are output photon-number distributions depending on phase shift ϕ, (b), (c) are output photon-number distributions for the Yurke state with bias phases $\phi = -1.46$ and $\phi = 0.00$, (g), (h) are output photon-number distributions for the classical state with bias phases $\phi = -1.63$ and $\phi = 0.05$ respectively. (d), (e) Show the dependence of the average, $\langle \hat{S}_1 \rangle (\phi)$ and the noise, $\Delta S_1^2 (\phi)$, on the bias phase at the output for the Yurke state, respectively. (i), (j) Show dependence of the average, $\langle \hat{S}_1 \rangle (\phi)$ and the noise, $\Delta S_1^2 (\phi)$, on the bias phase at the output for the classical state, respectively.

classical state does not show the oscillation (figure 3(g)), resulting in shot-noise at the output at the phase where the average is nearly zero (figure 3(h)).

For more detailed analysis, figures 3(d), (e), (i) and (j) show the averages and noises for S_1 for the Yurke state and uncorrelated photons, respectively. From the fitted curves, the phase derivative of the average output at $\phi = 0$, $|\partial \langle \hat{S}_1 \rangle / \partial \phi| |_{\phi=0} = 2.37$ and the noise at $\phi = 0$ is $\Delta S_1^2 (0) = 2.01$ for the Yurke state. Thus, the phase sensitivity by squeezing is $\delta \phi_{\mathrm{sq}} = 0.60$. Similarly, $|\partial \langle \hat{S}_1 \rangle / \partial \phi| |_{\phi=0} = 4.87$ and $\Delta S_1^2 (0) = 5.14$ and $\delta \phi_{\mathrm{coh.}} = 0.47$ for the classical uncorrelated case. Thus we obtained the noise reduction, which is the ratio of the $\Delta S_1^2 (0)$ of the Yurke state and the classical state, by a factor of 2.56. The phase sensitivity obtained using the Yurke state here did not exceed the theoretical shot-noise limit of $\delta \phi_{\mathrm{SNL}} = 1/\sqrt{5} \approx 0.45$ even though the output noise of the Yurke state is smaller than the shot noise $\xi_S = 0.63$.

To extract the maximum phase sensitivity, we calculated the phase sensitivity by using Fisher information obtained from equation (3) for the Yurke state. Figure 4 shows the bias phase dependence of Fisher information. The maximum of Fisher information is $F = 7.89$ at bias phase of $\phi = 0.21$ which is slightly different from the phase where the squeezing is maximum. Thus the obtained state can actually achieve sensitivity that is a factor of 1.58 smaller than the shot-noise limit. Note that maximum Fisher information is obtained at a slightly-different bias phase from where the squeezing is maximum. We can conclude that the improvement in the phase sensitivity is not only due to squeezing but also additional information reflected in the higher moments of the distributions [41]. In particular, Fisher information can extract the full information for changes in the phase parameter from the interference fringes at the output.

4. Conclusions

In conclusion, we have demonstrated, using our set-up, suppression of quantum noise by a factor of 2.56 with the effects of the squeezing being clearly shown by the measured interference fringes. Spin squeezing is often characterised using parameters ξ_S and ξ_R, where values <1 correspond to supra-classical performance. Our measurements show clear spin-squeezing using the parameter $\xi_s = 0.63$, while our measurements of ξ_R, which is traditionally used to quantify sub-shot noise phase-noise error in spin-squeezing experiments, is >1. None-the-less, the extracted Fisher information was 1.58 times better than shot-noise-limit demonstrating that quantum enhanced precision is possible even with $\xi_R \geqslant 1$. As an alternative to the multiplexed pseudo-number-counting detectors we used, recently-developed high-efficiency number-resolving detectors [42, 43] could be used to improve detection efficiency and therefore reduce measurement time. Our experimental demonstration is important not only for optical sub-shot-noise measurement but also other applications demonstrating sub-shot-noise spin-squeezed states [44–46].
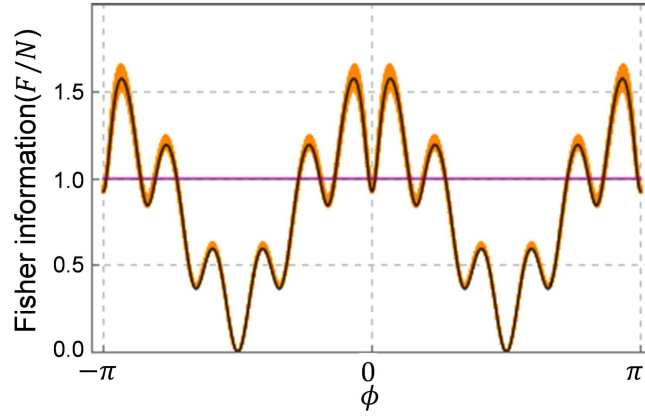
Figure 4. Fisher information extracted from interference fringes: the Fisher information for the Yurke state calculated using equation (3), from probability distributions which are fitted to the experimental data. The probability distributions are calculated using a model which incorporates mode mismatch and noise, and the fitting uses rescaled detector counts (see methods section). The purple line corresponds to the precision achievable at the shot-noise limit. The orange shading shows 200 iterations of a Monte-Carlo simulation, for which the Fisher information is computed with Poissonian noise added to raw detector counts.

We emphasise that since we only focus on the post-selected five photon events for this experiment, there are contributions to the output from lower photon-number states that are ignored, and the actual sensitivity is much lower if all these contributions are considered. To obtain actual quantum-enhanced sensitivity using Yurke states, we would need a deterministic or heralded source with fixed photon number. We note that the sensitivity using a setup for generating heralded two-photon Holland–Burnett states was reported and analysed in [47]. It is outstanding challenge to achieve heralded generation of Holland–Burnett states with high photon number, and furthermore this would need to be combined with single-photon subtraction to create Yurke states.

Note also that we did not make phase estimates using our model, but showed the possibility of improving the sensitivity by looking at the obtained probability distributions (as was done in [12, 13] for example). If the standard maximum-likelihood procedure were to be used to obtain phase estimates using our setup, individual estimates would each require tens or more counts to be accumulated. A comprehensive analysis of the statistics of these estimates, and therefore their sensitivity, would require thousands of such estimates to be obtained, which was not practical in our experiment due to coincidence counts of roughly 300 counts/8 h for each bias phase. We also remark that for the phase-estimation experiment reported in [15], it was shown that methods for measuring sensitivity using Fisher information derived from probability distributions, and maximum-likelihood estimation from simulated data (sampled from the same probability distributions) achieve close agreement.

5. Methods

5.1. Reconstruction of interference fringes for the Yurke state

Photon-number counts at our multiplexed detectors are analysed as follows. Single photons are detected at each APD with probabilities of σ_{a_i} ($i = 1, 2, \ldots 7$) in mode a and σ_{b_j} ($j = 1, 2, \ldots 7$) in mode b, which account for propagation loss and detector efficiency. In our analysis, we assume that five-fold coincidence detections arise only due to the generation of three photon pairs at the source (and neglect higher-order contributions). We define efficiency parameters for coincidence events at our multiplexed detectors as follows, where we assume that m clicks in path a and $5 - m$ clicks in path b correspond to m actual photons in a and $5 - m$ actual photons in path b:

$$
\begin{aligned}
\Sigma_m = &\sum_{x_{a_1}+\ldots+x_{a7}=m} m!\, \sigma_{a_1}^{x_{a_1}} \ldots \sigma_{a7}^{x_{a7}} \\
&\times \sum_{y_{b_1}+\ldots+y_{b7}=N-m} (5-m)!\, \sigma_{b_1}^{y_{b_1}} \ldots \sigma_{b_7}^{y_{b_7}},
\end{aligned}
\tag{5}
$$

where the variables $\{x_{a_i}\}$ and $\{y_{b_j}\}$ take values 0 or 1. To experimentally characterise Σ_m, we measured all of σ_{a_i} and σ_{b_j} (see table 1). Five-fold coincidence counts, $D_m(\phi_i)$, were then rescaled to give corrected count rates,

Table 1. Single-photon detection probabilities at individual APDs.

σ_{a_1}	σ_{a_2}	σ_{a_3}	σ_{a_4}	σ_{a_5}	σ_{a_6}	σ_{a_7}
1.40%	1.25%	1.43%	1.46%	1.53%	1.54%	1.48%
σ_{b_1}	σ_{b_2}	σ_{b_3}	σ_{b_4}	σ_{b_5}	σ_{b_6}	σ_{b_7}
1.16%	1.45%	1.30%	1.12%	1.11%	1.36%	1.58%

$$D'_m(\phi_i) = \frac{D_m(\phi_i)}{\Sigma_m},\tag{6}$$

To implement the data fitting, we use theoretically-derived probability distributions $P_{m,I}(\phi)$ which model mode-mismatch, where I is mode overlap between horizontal and vertical polarisations (see below). Our fittings minimise

$$\sum_{m=0}^{5}(M \times P_{m,I}(\phi) - D'_m(\phi_i))^2\tag{7}$$

using parameters ϕ, I and M, where M is a scaling parameter.

5.2. Derivation of probability distributions for the Yurke state including temporal mode mismatch
To derive $P_{m,I}(\phi)$, we start from theoretical model in [48]. The quantum state generated before the BS in figure 2 is given by

$$|\psi\rangle = \frac{(\hat{a}_{\mathrm{H}}^{\dagger})^{(N+1)/2}}{\sqrt{((N+1)/2)!}}\frac{(\hat{b}_{\mathrm{V}}^{\dagger})^{(N+1)/2}}{\sqrt{((N+1)/2)!}}|0\rangle.\tag{8}$$

$\hat{b}_{\mathrm{V}}^{\dagger}$ can be written as a superposition of one indistinguishable and one distinguishable component:

$$\hat{b}_{\mathrm{V}}^{\dagger} = \sqrt{I}\hat{a}_{\mathrm{V}}^{\dagger} + \sqrt{1-I}\hat{a}_{\mathrm{V}_{\perp}}^{\dagger},\tag{9}$$

where I is the indistinguishability given by $|\langle 0|\hat{a}_{\mathrm{H(V)}}\hat{b}_{\mathrm{H(V)}}^{\dagger}|0\rangle|^2$, and the symbol $\mathrm{V}_{\perp}$ denotes the orthogonal mode to H and V. In the following, we assume that modes $\hat{a}_{\mathrm{H(V)}}$ and $\hat{a}_{\mathrm{H_{\perp}(V_{\perp})}}$ do not interact so that we can consider reduced density matrix, $\hat{\rho}_{|\psi\rangle}$ where offdiagonal terms can be neglected as follows,

$$\hat{\rho}_{|\psi\rangle} = \sum_{d=0}^{(N+1)/2} C_d|(N+1)/2, (N+1)/2 - d\rangle\langle(N+1)/2, (N+1)/2 - d|_{\mathrm{HV}}$$
$$\otimes |d\rangle\langle d|_{\mathrm{V}_{\perp}},\tag{10}$$

where C_d is given by

$$C_d = \binom{(N+1)/2}{d}I(\tau)^{(N+1)/2-d}(1 - I(\tau))^d.\tag{11}$$

Replacing the annihilation operators for indistinguishable and distinguishable modes as

$$\hat{a}_{\mathrm{D}} = \frac{1}{\sqrt{2}}(\hat{a}_{\mathrm{H}} + \hat{a}_{\mathrm{V}}),$$
$$\hat{a}_{\mathrm{D}_{\perp}} = \frac{1}{\sqrt{2}}(\hat{a}_{\mathrm{H}_{\perp}} + \hat{a}_{\mathrm{V}_{\perp}}),\tag{12}$$

where D denotes diagonal polarisation, the state after the one-photon subtraction is given by a mixture of terms as follows,

$$\hat{\rho}_I = \frac{2}{N+1}(\hat{a}_{\mathrm{D}}\hat{\rho}_{|\psi\rangle}\hat{a}_{\mathrm{D}}^{\dagger} + \hat{a}_{\mathrm{D}_{\perp}}\hat{\rho}_{|\psi\rangle}\hat{a}_{\mathrm{D}_{\perp}}^{\dagger}).\tag{13}$$

The first term expresses the $(N+1)/2 + 1$ different distinguishability types and the second term expresses the $(N+1)/2$ different distinguishability types.

After the polarisation interferometer, the state is transformed as $\hat{\rho}_I(\phi) = \hat{U}(\phi)\hat{\rho}_I\hat{U}^{\dagger}(\phi)$ where $\hat{U}(\phi)$ is unitary transformation due to a half-wave plate, which is expressed as
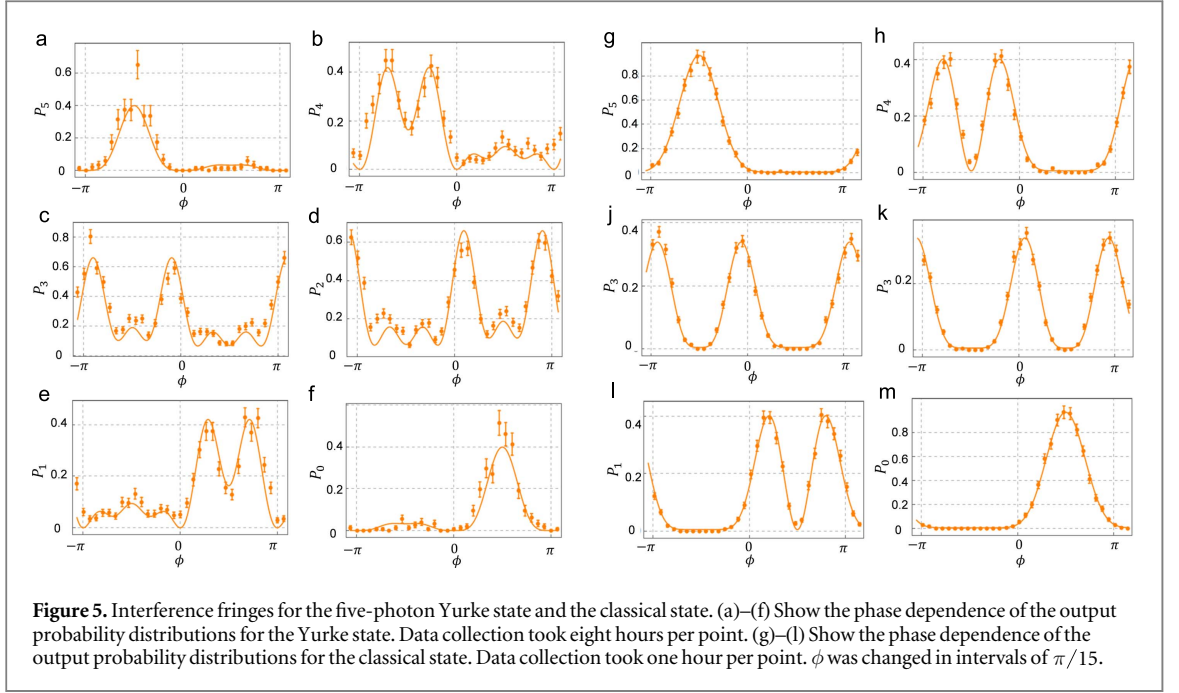
Figure 5. Interference fringes for the five-photon Yurke state and the classical state. (a)–(f) Show the phase dependence of the output probability distributions for the Yurke state. Data collection took eight hours per point. (g)–(l) Show the phase dependence of the output probability distributions for the classical state. Data collection took one hour per point. ϕ was changed in intervals of $\pi/15$.

$$\hat{U}(\phi)\hat{a}^{\dagger}_{H(H_{\perp})}\hat{U}(\phi) = \cos(\phi/2)\hat{a}^{\dagger}_{H(H_{\perp})} + \sin(\phi/2)\hat{a}^{\dagger}_{V(V_{\perp})},$$
$$\hat{U}(\phi)\hat{a}^{\dagger}_{V(V_{\perp})}\hat{U}^{\dagger}(\phi) = -\sin(\phi/2)\hat{a}^{\dagger}_{H(H_{\perp})} + \cos(\phi/2)\hat{a}^{\dagger}_{V(V_{\perp})}. \tag{14}$$

The probability that $N-m$ photons are detected in horizontally polarized mode and m photons are detected in vertically polarized mode is then given by

$$P_{m,I}(\phi) = \sum_{d=0}^{n}\sum_{s=0}^{d}\langle N-m-s, m-(d-s)|_{HV} \otimes \langle s, d-s|_{H_{\perp}V_{\perp}} \hat{\rho}_{I}(\phi)$$
$$\times |N-m-s, m-(d-s)\rangle_{HV} \otimes |s, d-s\rangle_{H_{\perp}V_{\perp}}, \tag{15}$$

which accounts for distinguishability with between 0 and n photons in the temporally-mismatched modes. As shown in figure 5, the probability functions given by equation (15) fit in accordance to the experimentally obtained data.

5.3. Calculation of Fisher information including phase insensitive noise

In spite of the accuracy of our theoretical model, some features in the interference fringes shown in figure 5 are not fully explained by the theory. Care must be taken as estimates of F are sensitive to perturbations in the fringes where there are extrema [15], as occurs for our experiment around $\phi = 0$. To ensure our estimates of F are robust (and do not overestimate the true value), we add a phase-insensitive noise to the functions $P_{m,I}(\phi)$ as follows,

$$P_{m,I,s}(\phi) = (1-s) \times P_{m,I}(\phi) + \frac{s}{6}, \tag{16}$$

where m takes values from 0 to 5.

Fisher information is then calculated using

$$F(\phi) = \sum_{m=0}^{5} P_{m,I,s}(\phi)\left(\frac{\partial}{\partial\phi}\ln P_{m,I,s}(\phi)\right)^{2}. \tag{17}$$

s was determined by fitting and the average value of s over 200 simulations was 0.085. F in figure 4 is computed using these modified distributions, which have lower values compared to the unmodified distributions around $\phi = 0$.

Note that the effect of imperfect indistinguishability derived in section 5.2 cannot explain the effect of this phase insensitive noise, which is roughly 8%. The phase-insensitive noise could arise from several factors, perhaps the most important being six-fold coincidence counts arising from components of the downconversion state with eight or more photons (and which have lost photons due to inefficiencies in the setup). However, the six-fold coincidence count rate (10^{-2}) in our current setup is too low to enable analysis of the effect of these higher-order contributions. This analysis would be done by repeating measurements over a range of pump power (or other gain parameter for the downconversion source) which we leave for future work. We also note

that the probability distributions derived by considering the effect of imperfect indistinguishability given by equation (15) can explain most of the features of experimental data as shown in figure 5.

Acknowledgments

References

[1] Giovannetti V, Lloyd S and Maccone L 2011 Advanced in quantum metrology *Nat. Photon.* **5** 222–9

[2] He Y M *et al* 2013 On-demand semiconductor single-photon source with near-unity indistinguishability *Nat. Nanotechnol.* **8** 213–7

[3] Vahlbruch H, Mehmet M, Danzmann K and Schnabel R 2016 Detection of 15 dB squeezed states of light and their application for the absolute calibration of photoelectric quantum efficiency *Phys. Rev. Lett.* **117** 110801

[4] Zoest T V *et al* 2010 Bose–Einstein condensation in microgravity *Science* **328** 1540

[5] Taylor M A *et al* 2013 Biological measurement beyond the quantum limit *Nat. Photon.* **7** 229–33

[6] Aasi J *et al* 2013 Enhanced sensitivity of the LIGO gravitational wave detector by using squeezed states of light *Nat. Photon.* **7** 613–9

[7] Bloom B J *et al* 2014 An optical lattice clock with accuracy and stability at the 10^{18} level *Nature* **506** 71–5

[8] Hosten O, Engelsen N J, Krishnakumar R and Kasevich M A 2016 Measurement noise 100 times lower than the quantum-projection limit using entangled atoms *Nature* **529** 505–8

[9] Caves C M 1981 Quantum-mechanical noise in an interferometer *Phys. Rev.* D **23** 1693

[10] Dowling J P 2008 Quantum optical metrology-the lowdown on high-N00N states *Contemp. Phys.* **49** 125

[11] Nagata T, Okamoto R, O'Brien J L, Sasaki K and Takeuchi S 2007 Beating the standard quantum limit with four-entangled photons *Science* **316** 726

[12] Afek I, Ambar O and Silberberg Y 2010 High-NOON states by mixing quantum and classical light *Science* **328** 879

[13] Xiang G Y, Hofmann H F and Pryde G J 2013 Optimal multi-photon phase sensing with a single interference fringe *Sci. Rep.* **3** 2684

[14] Kacprowicz M, Demkowicz-Dobrzański R, Wasilewski W, Banaszek K and Walmsley I A 2010 Experimental quantum-enhanced estimation of a lossy phase shift *Nat. Photon.* **4** 357–60

[15] Matthews J C F *et al* 2016 Towards practical quantum metrology with photon counting *npj Quantum Inf.* **2** 16023

[16] Higgins B L, Berry D W, Bartlett S D, Wiseman H M and Pryde G J 2007 Entanglement-free Heisenberg-limited phase estimation *Nature* **450** 393–6

[17] Birchall P M, O'Brien J L, Matthews J C F and Cable H 2016 The quantum–classical boundary for precision interferometric measurements arXiv:160207561v1

[18] Luis A and Korolkova N 2006 Polarization squeezing and nonclassical properties of light *Phys. Rev.* A **74** 043817

[19] Ono T and Hofmann H F 2008 Quantum enhancement of N-photon phase sensitivity by interferometric addition of down-converted photon pairs to weak coherent light *J. Phys. B: Mol. Opt. Phys.* **41** 095502

[20] Shalm L K, Adamson R B A and Steinberg A M 2009 Squeezing and over-squeezing of triphotons *Nature* **457** 67

[21] Beduini F A and Mitchell M W 2013 Optical spin squeezing: bright beams as high-flux entangled photon sources *Phys. Rev. Lett.* **111** 143601

[22] Rozema L A, Mahler D H, Blume-Kohout R and Steinberg A M 2014 Optimizing the choice of spin-squeezed states for detecting and characterizing quantum processes *Phys. Rev.* X **4** 041025

[23] Beduini F A *et al* 2015 Macroscopic quantum state analyzed particle by particle *Phys. Rev. Lett.* **114** 120402

[24] Pezzé L and Smerzi A 2009 Entanglement, nonlinear dynamics, and the Heisenberg limit *Phys. Rev. Lett.* **102** 100401

[25] Helstrom C W 1976 *Quantum Detection and Estimation Theory* (New York: Academic)

[26] Fisher R A 1925 Theory of statistical estimation *Proc. Camb. Phil. Soc.* **22** 700–25

[27] Kitagawa M and Ueda M 1993 Squeezed spin states *Phys. Rev.* A **47** 5138

[28] Ma J, Wang X, Sun C and Nori F 2011 Quantum spin squeezing *Phys. Rep.* **509** 89

[29] Appel J *et al* 2009 Mesoscopic atomic entanglement for precision measurements beyond the standard quantum limit *Proc. Natl. Acad. Sci.* **106** 10960

[30] Gross C, Zibold T, Nicklas E, Estève J and Oberthaler M K 2010 Nonlinear atom interferometer surpasses classical precision limit *Nature* **464** 1165

[31] Lücke B *et al* 2011 Twin matter waves for interferometry beyond the classical limit *Science* **334** 773

[32] Hamley C D, Gerving C S, Hoang T M, Bookjans E M and chman M S 2012 Spin-nematic squeezed vacuum in a quantum gas *Nat. Phys.* **8** 305

[33] Yurke B 1986 Input states for enhancement of fermion interferometer sensitivity *Phys. Rev. Lett.* **56** 1515

[34] Lee H, Kok P and Dowling P 2002 A quantum Rosetta stone for interferometry *J. Mod. Opt.* **49** 2325

[35] Hofmann H F 2006 Generation of a highly-phase-sensitive polarization-squeezed N-photon state by collinear parametric down-conversion and coherent photon subtraction *Phys. Rev.* A **74** 013808

[36] Wineland D J, Bolinger J J, Itano W M, Moore F L and Heinzen D J 1992 Spin squeezing and reduced quantum noise in spectroscopy *Phys. Rev.* A **46** R6797(R)

[37] Wineland D J, Bolinger J J, Itano W M and Heinzen D J 1994 Squeezed atomic states and projection noise in spectroscopy *Phys. Rev.* A **50** 67

[38] Casella G and Berger R L 2001 *Statistical Inference* (California: Duxbury)

[39] Hofmann H F 2009 All path-symmetric pure states achieve their maximal phase sensitivity in conventional two-path interferometry *Phys. Rev.* A **79** 033822

[40] Mehmet M, Vahlbruch H, Lastzka N, Danzmann K and Schnabel R 2010 Observation of squeezed states with strong photon-number oscillations *Phys. Rev.* A **81** 013814

[41] Strobel H *et al* 2015 Fisher information and entanglement of non-Gaussian spin states *Science* **345** 424

[42] Takeuchi S, Kim J, Yamamoto Y and Hogue H H 1999 Development of a high-quantum-efficiency single-photon counting system *Appl. Phys. Lett.* **74** 1063

[43] Humphreys P C *et al* 2015 Tomography of photon-number resolving continuous-output detectors *New J. Phys.* **17** 103044

[44] Amico L, Fazio R, Osterloh A and Vedral V 2008 Entanglement in many-body systems *Rev. Mod. Phys.* **80** 517

[45] Horodecki R, Horodecki P, Horodecki M and Horodecki K 2009 Quantum entanglement *Rev. Mod. Phys.* **81** 865

[46] Guehne O and Tóth G 2009 Entanglement detection *Phys. Rep* **474** 1

[47] Thomas-Peter N *et al* 2011 Real-world quantum sensors: evaluating resources for precision measurement *Phys. Rev. Lett.* **107** 113603

[48] Ra Y-S *et al* 2013 Observation of detection-dependent multi-photon coherence times *Nat. Commun.* **4** 2451

[49] Sabines-Chesterking J, Cable H, Ono T, Matthews J C F and O'Brien J L 2017 Optical implementation of spin squeezing https://data.bris.ac.uk/data/dataset/1u56e9gm6h2ao2iqlv9mkd7zd7 (Accessed: 11 May 2017)